Cell Reports
Report

Retrograde Synaptic Signaling Mediated by K^+ Efflux through Postsynaptic NMDA Receptors

Pei-Yu Shih,[1] Leonid P. Savtchenko,[2] Naomi Kamasawa,[3,5] Yulia Dembitskaya,[1,4] Thomas J. McHugh,[1] Dmitri A. Rusakov,[2] Ryuichi Shigemoto,[3] and Alexey Semyanov[1,4,*]
[1]RIKEN Brain Science Institute, Wako, Saitama 351-0198, Japan
[2]UCL Institute of Neurology, University College London, London WC1N 3BG, UK
[3]National Institute for Physiological Sciences, Myodaiji, Okazaki 444-8787, Japan
[4]University of Nizhny Novgorod, Nizhny Novgorod 603950, Russia
[5]Present address: Max Planck Florida Institute, Jupiter, FL 33458, USA
*Correspondence: semyanov@brain.riken.jp
http://dx.doi.org/10.1016/j.celrep.2013.10.026

SUMMARY

Synaptic NMDA receptors (NMDARs) carry inward Ca^{2+} current responsible for postsynaptic signaling and plasticity in dendritic spines. Whether the concurrent K^+ efflux through the same receptors into the synaptic cleft has a physiological role is not known. Here, we report that NMDAR-dependent K^+ efflux can provide a retrograde signal in the synapse. In hippocampal CA3-CA1 synapses, the bulk of astrocytic K^+ current triggered by synaptic activity reflected K^+ efflux through local postsynaptic NMDARs. The local extracellular K^+ rise produced by activation of postsynaptic NMDARs boosted action potential-evoked presynaptic Ca^{2+} transients and neurotransmitter release from Schaffer collaterals. Our findings indicate that postsynaptic NMDAR-mediated K^+ efflux contributes to use-dependent synaptic facilitation, thus revealing a fundamental form of retrograde synaptic signaling.

INTRODUCTION

Activity-dependent regulation of synaptic transmission often involves both pre and postsynaptic cells releasing neurotransmitters and neuromodulators. At central excitatory synapses, released glutamate can modulate presynaptic activity by targeting presynaptic metabotropic glutamate receptors (mGluRs) (Gereau and Conn, 1995), kainate receptors (Contractor et al., 2011), and, at least in developing tissue, NMDA receptors (NMDARs) (Corlew et al., 2007; McGuinness et al., 2010). Another common regulatory mechanism involves the activity-dependent release of retrograde messengers from the postsynaptic neuron, including endocannabinoids, growth factors, nitric oxide, and conventional neurotransmitters (reviewed in Regehr et al., 2009). However, these mechanisms rely on organic signaling molecules, and the impact of activity-dependent ionic changes within the narrow synaptic cleft has received much less attention. For example, activation of postsynaptic NMDARs could prompt partial extracellular Ca^{2+} depletion, thus reducing, at least for a very brief period of time, synaptic release probability at hippocampal CA3-CA1 synapses (Rusakov and Fine, 2003). Local extracellular K^+ can rise both during action potentials (APs) and during excitatory postsynaptic potentials (EPSPs) (Ge and Duan, 2007; Nicholson et al., 1978; Poolos et al., 1987; Prince et al., 1973), with its average concentration growing 2-fold during intense neuronal discharges (Krnjević et al., 1982). Although during moderate physiological activity external K^+ increases rarely exceed 0.2–0.4 mM, these commonly reported values are averaged over space and time. In fact, K^+ elevations in the local vicinity of K^+ sources, such as K^+-permeable receptors and channels, could theoretically attain much higher levels. These hot spots of extracellular K^+ could potentially occur in the synaptic cleft, thus affecting synaptic function. In this study, we explore hippocampal circuitry to test this hypothesis. We find that postsynaptic NMDARs are a major source of K^+ in the synaptic cleft that affects presynaptic release probability, thus suggesting an additional form of retrograde synaptic signaling.

RESULTS

Activation of Postsynaptic NMDARs Produces Local K^+ Elevations

K^+ released during network activity is cleared mainly through astrocytic electrogenic uptake (Walz, 2000). We therefore monitored extracellular K^+ dynamics by recording astrocytic currents in response to electrical stimulation of Schaffer collaterals in murine hippocampal slices (Figures 1A and 1B). In the presence of $GABA_A$, $GABA_B$, mGluR, and AMPA receptor (AMPAR) antagonists, stimulation triggered a biphasic inward current. The fast component of this current represents glutamate uptake, whereas its slow component reflects K^+ influx (Bergles and Jahr, 1997). Indeed, bath application of 200 μM $BaCl_2$, which blocks inward rectifier K^+ channel, strongly inhibited the slow current component (hereafter termed I_K; 85 ± 25.6 pA for control [Ctrl], 7 ± 1.7 pA for $BaCl_2$, $n = 5$; $p < 0.05$, Wilcoxon signed-rank test; Figure 1B). The fast component was suppressed by the glutamate transporter inhibitor DL-threo-β-benzyloxyaspartic acid (TBOA;

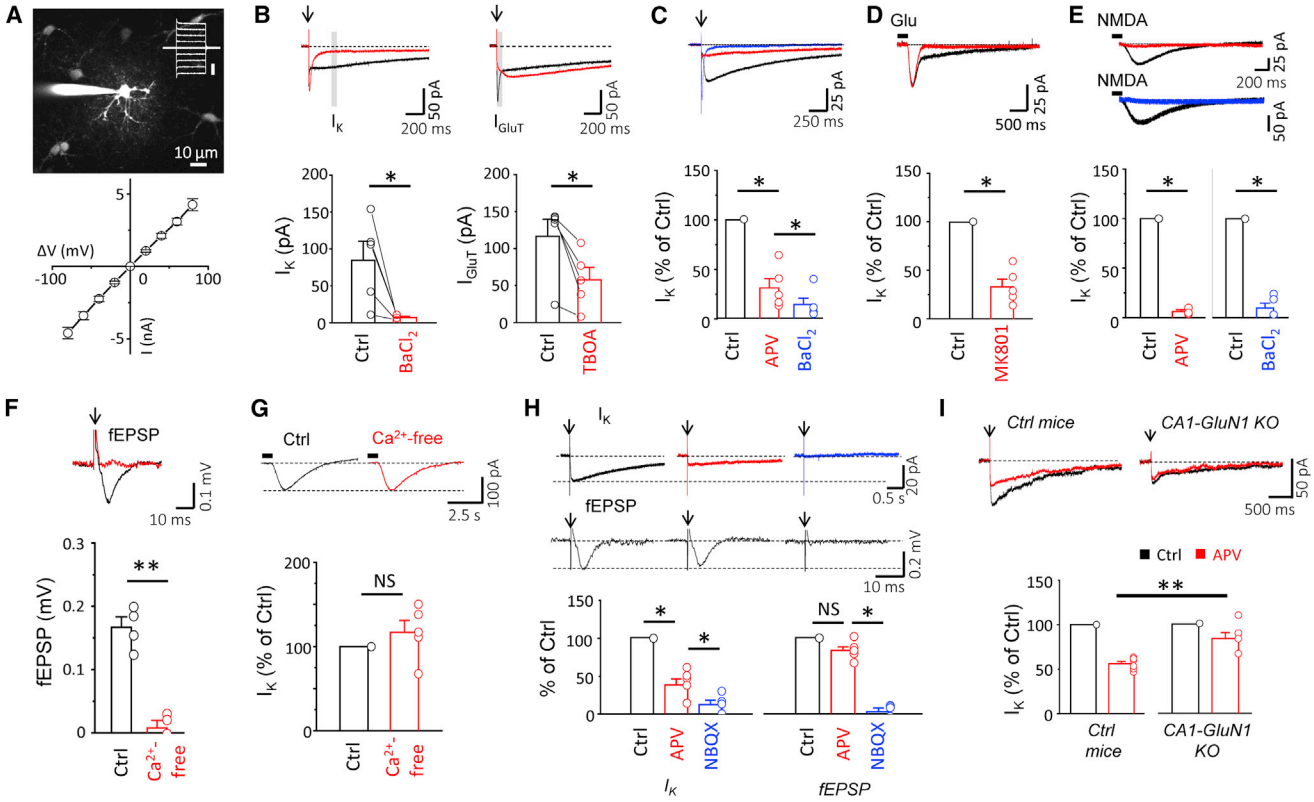

Figure 1. Postsynaptic NMDARs Mediate K^+ Efflux

(A) Recording from "passive" astrocyte in hippocampal slice is presented. Top view shows the astrocyte loaded with fluorescent dye Alexa Fluor 594 through the patch pipette, through which depolarizing pulses were delivered. Bottom view shows linear I–V curve, characteristic to "passive" astrocyte.

(B) Left view shows that $BaCl_2$ blocked the slow component (I_K) of the synaptically induced current in astrocytes. Right view shows that TBOA blocked the fast component (I_{GluT}). Top views are sample traces in Ctrl (black) and in drug (red). Gray vertical bar indicates the time point where the corresponding current was measured. Bottom views are summary plots.

(C) Synaptically induced I_k is suppressed by APV. Top view is sample traces in Ctrl (black), in APV (red) and in $BaCl_2$ (blue). Bottom view is summary plot of consecutive APV and $BaCl_2$ applications on I_K.

(D) I_k induced by L-glutamate puff was suppressed by MK801. Top view is sample traces in Ctrl (black) and MK801 (red). Bottom view is a summary plot of MK801 effect on I_K.

(E) I_k induced by NMDA puff was suppressed either by APV or $BaCl_2$. Top view is sample traces in Ctrl (black), APV (red), and $BaCl_2$ (blue). Bottom view is summary plots of APV and $BaCl_2$ effects on I_K.

(F) Ca^{2+} removal (Ca^{2+}-free) suppresses synaptic transmission. Top view is fEPSP in Ctrl (black) and in Ca^{2+}-free solution (red). Bottom view is summary plots.

(G) There was no significant effect of Ca^{2+} removal on I_K induced by NMDA puff. Top view is sample traces in Ctrl (black) and Ca^{2+}-free solution (red). Bottom view is summary plot.

(H) Effects of consecutive APV and NBQX applications on fEPSP and I_K were recorded simultaneously. Top view is sample traces in Ctrl (black), APV (red), and NBQX (blue). Bottom view is summary plots.

(I) Reduced effect of APV on synaptically induced I_K in CA1-GluN1 KO mice compared to Ctrl mice is shown. Top views are sample traces in Ctrl (black) and APV (red). Bottom views are summary plots of APV effect in CA1-GluN1 KO and Ctrl mice.

Columns represent the mean, circles the individual slices. Error bars, SEM. Not significant (NS) $p > 0.05$, *$p < 0.05$, and **$p < 0.01$. Arrows indicate synaptic stimulation. Horizontal black bars next to sample traces represent the agonist puff.

See also Figure S1.

50 μM) (I_{GluT}: 117 ± 23.2 pA for Ctrl and 58 ± 16.9 pA for TBOA, $n = 5$; $p < 0.05$, Wilcoxon signed-rank test; Figure 1B). Surprisingly, the Ba^{2+}-sensitive I_K was also significantly suppressed by APV (50 μM), a NMDAR antagonist (69% ± 9.4% peak reduction, $n = 5$; $p < 0.05$, Wilcoxon signed-rank test; Figure 1C). GluN1 subunits, which are required for functional NMDARs, are not expressed in hippocampal astrocytes (Krebs et al., 2003), indicating that this portion of I_K is mediated by neuronal NMDARs. This I_K suppression was not due to the reduced recruitment of afferent Schaffer collaterals because APV had no significant effect on the presynaptic fiber volley (PrV; 105% ± 3.8% of Ctrl, $n = 15$; $p = 0.52$, Wilcoxon signed-rank test; Figure S1). Furthermore, in the presence of tetrodotoxin (TTX; 1 μM, Na^+ channel blocker), puff application of glutamate (400 μM) produced a biphasic current with the slow component abolished by MK801 (10 μM), another NMDAR antagonist (ΔI_K: 90% ± 4.8% peak reduction, $n = 5$; $p < 0.05$, Wilcoxon signed-rank test; Figure 1D). Finally, puff application of NMDA (1 mM), a nontransported

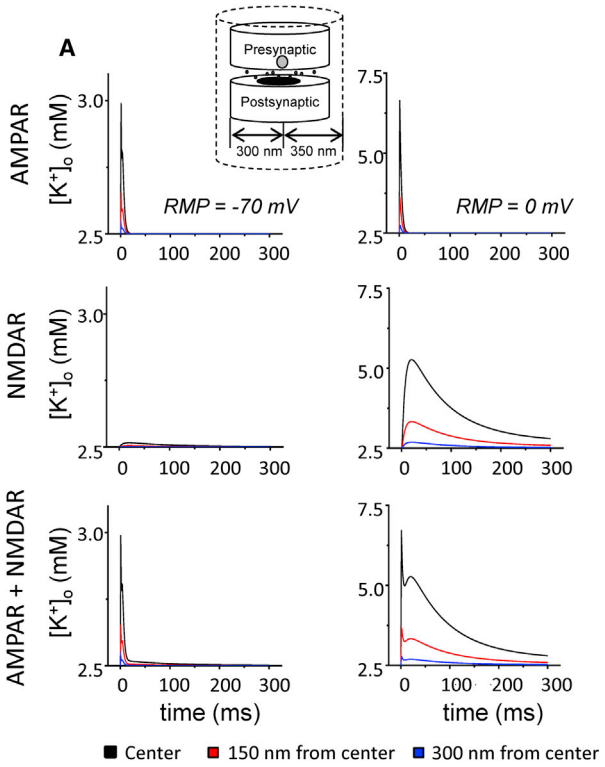

Figure 2. Model of K^+ Dynamics in the Synaptic Cleft

(A) Simulated time course of K^+ concentration $[K^+]_o$ inside the synaptic cleft is shown. Black traces indicate the time course in the center of the cleft, red at 150 nm from the center, and blue at 300 nm from the center. See Experimental Procedures for modeling details. Left column of the graphs is simulation at an RMP of −70 mV, right column is simulation at a RMP of 0 mV. Top row shows synapse containing 50 AMPARs, middle containing 20 NMDARs, and bottom containing 50 AMPAR and 20 NMDARs. Inset is the schematics of the model synapse.

(B) The maximum $[K^+]_o$ at the center of synaptic cleft was simulated for synapses with different receptor content (white circles indicate 50 AMPARs, gray circles 20 NMDARs, and black circles 50 AMPARs and 20 NMDARs) at different RMPs.

(C) The total number of K^+ ions passing through NMDARs and AMPARs during EPSC depending on RMP is shown. Notations are the same as in (B).

(D) Peak conductance of 20 NMDARs and 50 AMPARs at different RMP is presented. Notations are the same as in (B).

NMDAR agonist, induced a single-phase, Ba^{2+}-sensitive I_K that was blocked by APV (ΔI_K: 94% ± 1.9% peak reduction by APV, n = 3; ΔI_K: 90% ± 4.8% peak reduction by Ba^{2+}, n = 5; $p < 0.05$, Wilcoxon signed-rank test; Figure 1E). Taken together, these results indicate that a substantial component of astrocytic I_K was due to activation of neuronal NMDARs.

Although NMDARs are permeable to K^+ (Ichinose et al., 2003), Ca^{2+} influx through these receptors also can activate Ca^{2+}-dependent K^+ (K_{Ca}) channels (Ngo-Anh et al., 2005), and in addition, the depolarizing action of NMDARs can engage voltage-dependent K^+ (K_V) channels (Qiu et al., 2007). We first tested the contribution of K_{Ca} to I_K (in these experiments, synaptic receptors were left unblocked). Removal of extracellular Ca^{2+} abolished field EPSPs (fEPSPs; 3% ± 6.9% of Ctrl, n = 4; Figure 1F) but had no significant effect on I_K induced by a puff of 1 mM NMDA (I_K: 117% ± 14.2% of Ctrl, n = 5; p = 0.31, Wilcoxon signed-rank test; Figure 1G), arguing against a significant contribution of K_{Ca} channels. Second, if NMDARs activate K_V channels via postsynaptic depolarization, I_K should vary consistently with fEPSPs. To test this, we performed simultaneous astrocyte and fEPSP recordings. As expected, fEPSPs depended mainly on AMPAR activation (blocking NMDARs with APV decreased the fEPSP amplitude only to 83% ± 4.6% of Ctrl; this current was effectively abolished by subsequent application of 25 μM NBQX, AMPAR antagonist; 2% ± 4.9% of Ctrl, n = 5; p = 0.19 for APV effect and $p < 0.05$ for NBQX effect, Wilcoxon signed-rank test; Figure 1H). In striking contrast, blocking NMDARs with APV suppressed astrocytic I_K substantially (I_K decreased to 38% ± 8.0% of Ctrl, n = 5; $p < 0.05$, Wilcoxon signed-rank test; Figure 1H). If depolarization were to directly translate to K^+ efflux through activation of K_V channels, then both fEPSP and I_K would be decreased proportionately. Thus, these results suggest that NMDAR-dependent depolarization per se provides only a minor, if any, contribution to the NMDAR-mediated K^+ efflux. Notably, subsequent addition of NBQX resulted in further reduction of I_K (I_K: 12% ± 5.9% of ctrl, n = 5; $p < 0.05$ for difference with APV effect, Wilcoxon signed-rank test; Figure 1H).

We next asked if the NMDARs responsible for the K^+ efflux are located pre- or postsynaptically, by taking advantage of a transgenic mouse line (CA1-GluN1 knockout [KO]) that conditionally deletes GluN1 in a large proportion of postsynaptic CA1 pyramidal neurons, but not in presynaptic CA3 pyramidal neurons (Tsien et al., 1996). Consistent with the predominant contribution of postsynaptic NMDARs in raising intracleft K^+, I_K induced by afferent stimulation was almost three times less sensitive to APV in the KO animals (I_K, 16% ± 6.6% reduction; n = 6) than in Ctrl littermates (I_K: 44% ± 2.7% reduction, n = 6; $p < 0.01$ for difference with CA1-GluN1 KO, unpaired t test, single tailed; AMPARs were left unblocked, which could explain additional K^+ efflux in these experiments, Figure 1I).

K^+ Dynamics in the Synaptic Cleft

Therefore, our results are consistent with the notion that K^+ efflux during synaptic signaling was mediated by both NMDARs and AMPARs (Bergles and Jahr, 1997; Ge and Duan, 2007). However, despite the larger number of AMPARs per synapse, the contribution of NMDARs to K^+ efflux could be greater because of their longer open times. To test this theoretically, we investigated K^+ dynamics in synaptic cleft using a previously tested realistic model of intracleft diffusion at CA3-CA1 synapses (Figure 2A) (Savtchenko and Rusakov, 2007; Savtchenko

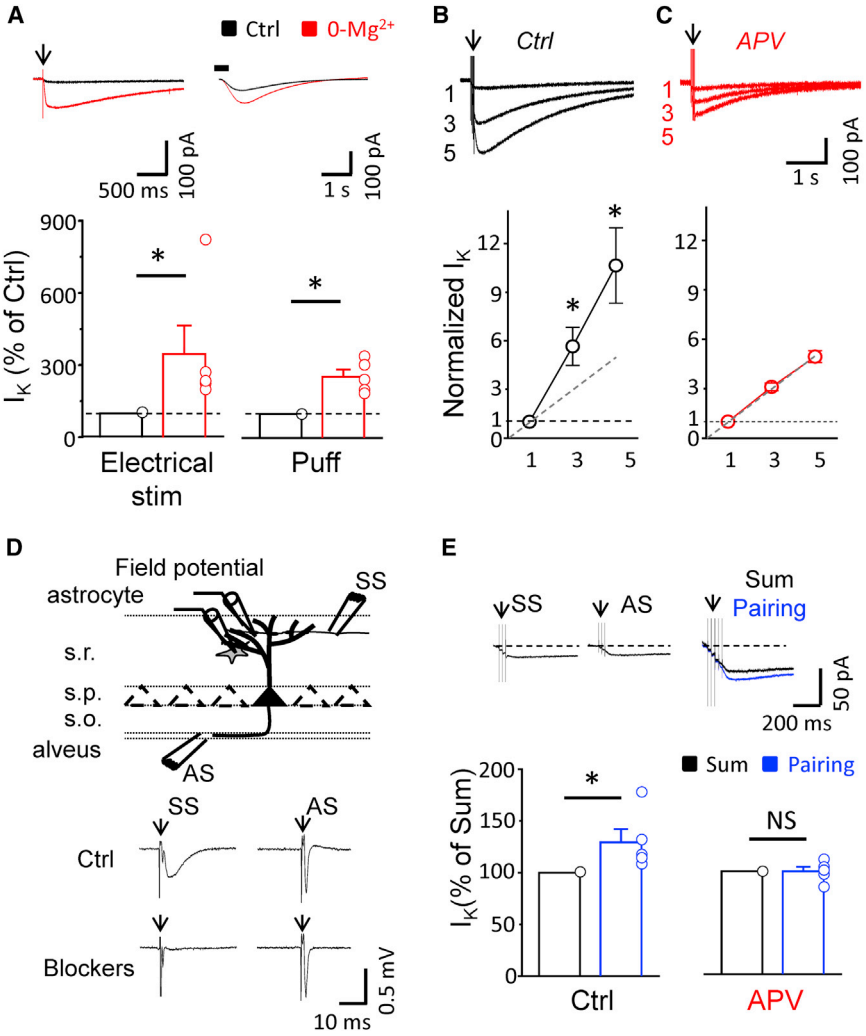

Figure 3. Activity Dependence of NMDARs Mediated K^+ Efflux

(A) Mg^{2+} removal enhanced I_K induced either by electrical stimulation (left) or NMDA puff (right). Top views are sample traces in Ctrl (black) and in 0-Mg^{2+} (red), Bottom views are summary plots.

(B and C) NMDAR-dependent supralinear increase of I_K with one, three, and five stimuli at 50 Hz is shown. Top views are sample traces in Ctrl (B, black) and in APV (C, red), Bottom views are summary plots. Dashed line indicates linear sum.

(D) Top view is a schematic showing electrodes' positions for SS, AS, extracellular field potential recording, and astrocytic I_K recording. Bottom view is sample traces of field potential recordings in response to SS (fEPSP) and AS (antidromic population spike). Synaptic receptor blockers suppressed fEPSP, but not antidromic population spike.

(E) Pairing of SS (three stimuli, 50 Hz) and AS (three stimuli, 50 Hz) produced supralinear summation of I_K. Top views are sample traces of I_K in response to SS, AS, arithmetic sum, and pairing (blue). Bottom views are summary plots in Ctrl and in APV. Columns represent the mean, circles the individual slices. Error bars, SEM. NS $p > 0.05$ and $^*p < 0.05$. Arrows indicate electrical stimulation. Horizontal black bars indicate agonist puff.

See also Figure S2.

et al., 2013). The model incorporated a 200 nm wide postsynaptic density containing 50 AMPARs and/or 20 NMDARs. The key parameter of simulations, i.e., the number of GluN1-containing NMDARs, was experimentally estimated at 394 particles/μm^2 in a separate study by counting the average density of postsynaptic receptors immunolabeled in SDS-digested freeze fracture replica labeling (SDS-FRL, see sections below for details). We investigated K^+ dynamics inside the synaptic cleft following release of 3,000 glutamate molecules (Savtchenko et al., 2013), mimicking conditions of the current clamp. When the cell was initially at a V_m of −70 mV, the activation of local AMPARs alone produced a larger peak increase in the intracleft K^+ compared to NMDARs (Figures 2A and 2B). However, integrated K^+ efflux was similar for AMPAR and NMDAR activation because of the prolonged activation time course of NMDARs (Figure 2C). This scenario changed dramatically upon postsynaptic depolarization that relieved the Mg^{2+} block of NMDARs. When basal V_m was set to zero, the number of NMDARs activated during glutamate release sharply increased, boosting local K^+ efflux orders of magnitude (Figure 2D). This result suggests that postsynaptic cell depolarization during repetitive activation could lead to substantial NMDAR-dependent K^+ elevation in the synaptic cleft.

NMDAR-Mediated K^+ Efflux Depends on Activity of the Postsynaptic Cell

The model predicts that removal of voltage-dependent Mg^{2+} block of NMDARs should substantially enhance K^+ efflux, and in physiological conditions, this block is at least partly relieved through AMPAR-dependent local EPSP. Nevertheless, removal of extracellular Mg^{2+} increased both the I_K induced by either electrical stimulation of Schaffer collaterals (to 346% ± 118.5% of Ctrl, n = 5; $p < 0.05$, Wilcoxon signed-rank test; Figure 3A) or a NMDA puff (to 256% ± 30% of Ctrl, n = 5; $p < 0.05$, Wilcoxon signed-rank test; Figure 3A). We tested whether progressively boosting postsynaptic depolarization by repetitive cell excitation could have a similar effect. We found that during brief bursts of synaptic discharges, the I_K amplitude increased dramatically: 5.6 ± 1.2 times with three stimuli and 10.6 ± 2.3 times with five stimuli (n = 9; p = 0.02 for difference with linear sum for three stimuli and p = 0.01 for five stimuli, Wilcoxon signed-rank test; Figure 3B). This large supralinear enhancement was completely blocked by APV (normalized amplitude of I_K was 3.1 ± 0.2 with three stimuli and 4.9 ± 0.4 with five stimuli, n = 6; p = 0.34 for difference with linear sum for three stimuli and p = 0.57 for five stimuli, Wilcoxon signed-rank test, Figure 3C), suggesting that it indeed requires NMDARs.

Because NMDARs can also be unblocked, albeit only briefly, by bAPs (Schiller et al., 1998; Wu et al., 2012), we tested if

bAPs enhance I_K in response to stimulation of Schaffer collaterals (SS). bAPs were induced by antidromic stimulation (AS) with an extracellular electrode placed on the border between *str.oriens* and *alveus* (Figure 3D). In the absence of synaptic receptor blockers, SS induced a fEPSP, whereas AS induced antidromic population spike. This fEPSP was suppressed by a cocktail of AMPA, mGluR, and GABA receptor blockers, whereas the antidromic population spike remained. SS (3 × 50 Hz) and AS (3 × 50 Hz) were delivered first separately, then paired. The pairing of SS and AS produced an I_K that was significantly larger than the arithmetic sum of the I_K produced by SS and AS alone: I_K(pairing) was 129% ± 12.6% of I_K(sum) (n = 5; $p < 0.05$, Wilcoxon signed-rank test; Figure 3E). The enhancement of I_K by pairing was abolished by APV: 99.8% ± 4.5% of I_K(sum) ($p = 0.50$, Wilcoxon signed-rank test; Figure 3E). Thus, depolarization of the postsynaptic cell by bAP can boost NMDAR-mediated K^+ efflux. This may be an important mechanism that aids synaptic depolarization (e.g., when only single synapse is activated; see below). However, if depolarization is mediated by multiple synapses, the coinciding EPSP and bAP may not necessarily produce a supralinear increase in K^+ efflux due to occlusion (e.g., multisynaptic EPSP can trigger APs by themselves). Indeed, this was the case when we repeated the pairing experiment without blocking synaptic receptors (Figure S2). Taken together, these results indicate that K^+ efflux through NMDARs is significantly boosted by postsynaptic activity.

NMDAR-Mediated K^+ Efflux Enhances Presynaptic Ca^{2+} Entry

Although our data suggest that K^+ efflux has no significant effect on the Schaffer collateral fiber volley (Figure S1), this does not rule out its local depolarizing effects on presynaptic boutons. The depolarization-dependent widening of local presynaptic APs in the boutons could lead to increases in presynaptic Ca^{2+} entry (Geiger and Jonas, 2000; Hori and Takahashi, 2009; Sasaki et al., 2011). To test if this is the case, we used two-photon Ca^{2+} imaging in axonal boutons of CA3 pyramidal neurons loaded with 50 μM Ca^{2+}-insensitive dye Alexa Fluor 594 and 200 μM Ca^{2+}-sensitive Fluo-5F, as described recently by Sylantyev et al. (2013) (Figures 4A and 4B). The Ca^{2+} transients were induced by APs that were triggered in soma by brief current injections and were recorded as the change in the Ca^{2+}-sensitive G channel fluorescence over Ca^{2+}-insensitive R channel fluorescence level (ΔG/R). The experiments were performed in the absence of all blockers. To minimize the effects of slow dye equilibration across long axons, recordings with pharmacological treatments were normalized against mean Ca^{2+} transients recorded at matching time points in Ctrl experiments (Sylantyev et al., 2013) (see Experimental Procedures). Surprisingly, we found that blocking NMDARs by APV had no effect on Ca^{2+} transients elicited by 5 × 50 Hz APs (ΔG/R: 97.9% ± 7.3% of Ctrl recordings, n = 5; $p = 0.41$, unpaired t test; Figure 4C). It is possible that the activation of only one presynaptic axon (because only one presynaptic cell was stimulated in these experiments) produces a monosynaptic EPSP that is insufficient to substantially relieve the Mg^{2+} block among postsynaptic NMDARs. Indeed, most Schaffer collaterals (76%) make a single apposition on a CA1 pyramidal neuron, and only an additional 4% of the axons wind back and forth across individual dendrites, forming multiple closely spaced synapses (Sorra and Harris, 1993). To test the effects of further Mg^{2+} block relief on NMDAR-dependent presynaptic Ca^{2+} entry (such as during multisynaptic EPSPs exerting strong postsynaptic depolarization), we removed Mg^{2+} from perfusion solution (NBQX was added in this case to prevent epileptiform activity). Indeed, Mg^{2+}-free solution significantly enhanced presynaptic Ca^{2+} entry produced by activation of a single axon (ΔG/R: 119.0% ± 6.1% of Ctrl recordings, n = 7; $p < 0.05$, unpaired t test; Figure 4D). This enhancement was abolished by APV (ΔG/R: 103.9% ± 5.6% of Ctrl recordings, n = 7; $p = 0.31$, unpaired t test; Figure 4D), suggesting that NMDARs modulate presynaptic Ca^{2+} entry if a sufficient number of these receptors are enabled. Then, we added MK801 to the patch-pipette solution (iMK801) to block presynaptic NMDARs intracellularly (see Figure S3 for Ctrl effects of iMK801 on synaptically induced NMDAR responses) and found that in these conditions, the removal of extracellular Mg^{2+} was still able to potentiate presynaptic Ca^{2+} transients elicited by 5 × 50 Hz APs (ΔG/R: 120.8% ± 4.6% of Ctrl recordings, n = 9; $p < 0.05$, unpaired t test; Figure 4E), suggesting that the observed potentiation does not require presynaptic NMDARs.

In developing tissue, the modulation of presynaptic Ca^{2+} transients by NMDARs can be attributed to presynaptic NMDARs (Corlew et al., 2007; McGuinness et al., 2010). We therefore investigated the expression of presynaptic NMDARs in rats at P26 using the immunoelectron-labeling methodology, SDS-FRL (Tarusawa et al., 2009), which can directly separate images of pre- and postsynaptic membranes in the CA1 region of the hippocampus. Presynaptic active zones were identified by immunolabeling for the CAZ-associated structural protein (CAST) on the P face of complementary images (Figure 4F; see Experimental Procedures). When the fracture plane occurred in a synapse, the presynaptic P face was labeled for CAST, and the postsynaptic E face was labeled for GluN1, and both were observed adjacent to each other. In the examined replicas, the labeling density of the postsynaptic GluN1 was 394 ± 194 μm^{-2}. Out of 49 presynaptic active zones with CAST labeling on the P face, 48 had no labeling for GluN1 on the complementary E face of the synapse (Figure 4F). This result suggests that presynaptic NMDARs occur inside active zones at only ~2% CA1 synapses at this age, and thus, the contribution of presynaptic NMDARs to the modulation of presynaptic Ca^{2+} transients in imaged boutons is, if anything, unlikely.

NMDAR-Mediated K^+ Efflux Boosts Ca^{2+}-Dependent Glutamate Release

To further test if the activation of NMDARs during stimulation of multiple axons can affect presynaptic Ca^{2+} transients, we bolus loaded Schaffer collaterals with a membrane-permeable Ca^{2+} dye, Oregon green BAPTA-1 AM, and recorded Ca^{2+} transients in labeled boutons ~200 μm away from the loading site (Figures 5A and 5B). Under these conditions (multiaxon stimulation in the absence of all blockers), Ca^{2+} transients (fluorescence increment ΔF/F) evoked by extracellular stimulation (5 × 50 Hz) were significantly reduced by APV application, to 80.7% ± 12.2% of baseline (n = 12; $p < 0.05$, Wilcoxon signed-rank test; Figure 5C).

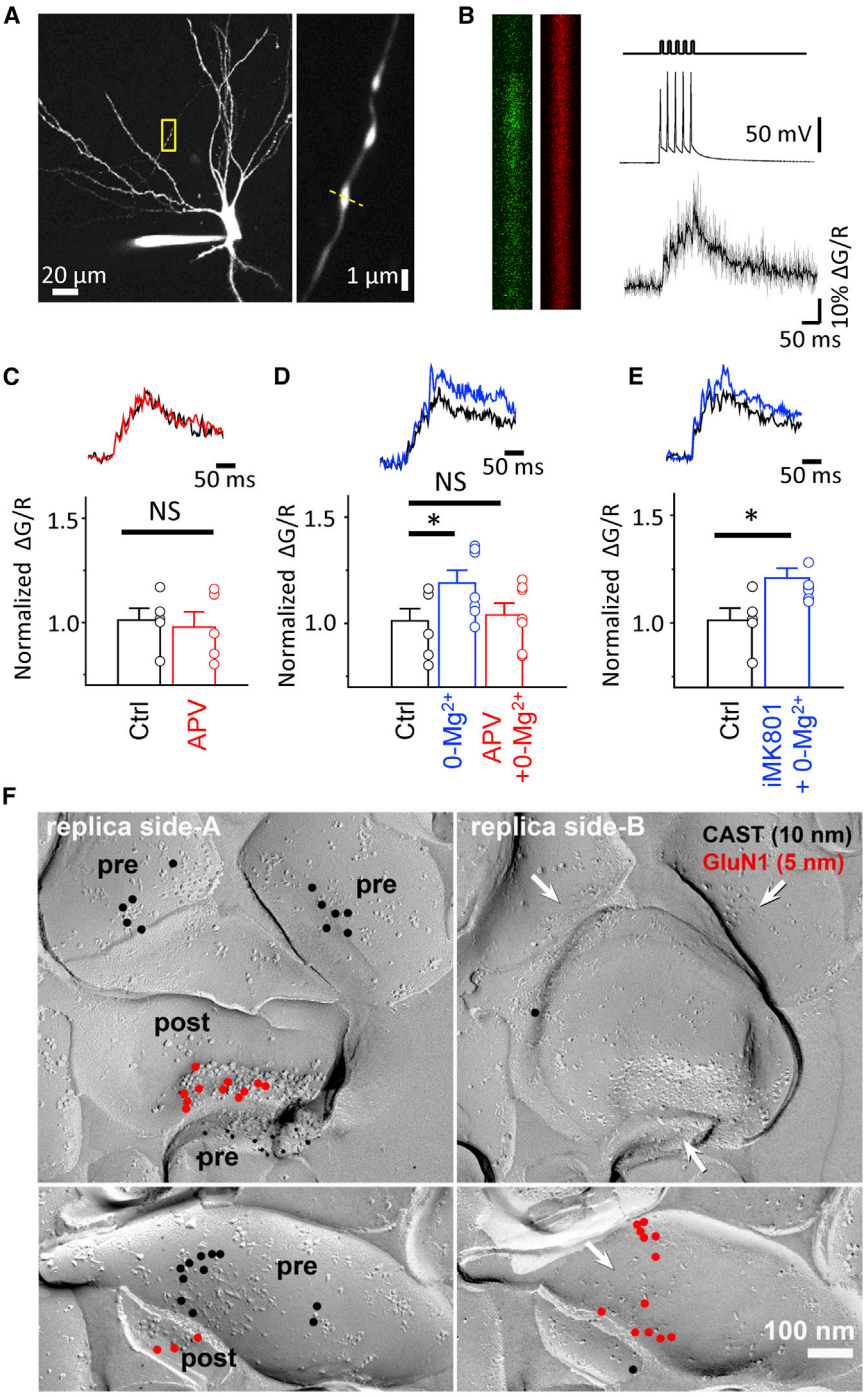

Figure 4. Postsynaptic NMDARs Regulate Presynaptic Ca^{2+} Transients

(A) The left panel is a two-photon image showing a CA3 pyramidal neuron loaded with Alexa Fluor 594. Right panel is a close-up image of the axon with boutons boxed on the left. Yellow dotted line indicates place of line scan.

(B) Sample of line-scan images of Fluo-5F (green) and Alexa Fluor 594 (red) is presented. Changes in Fluo-5F are produced by APs evoked in soma (five stimuli, 50 Hz). Arrow points to the start of the stimulation. Traces on the right are current pulse injections in soma, AP recorded in soma, and Ca^{2+} transients in axonal bouton (ΔG/R, gray indicates six individual traces and averaged thick black trace).

(C) APV did not produce significant change in presynaptic Ca^{2+} transients in individual boutons. Top view is sample traces. Black indicates Ctrl, red APV. Bottom view is summary plots.

(D) Mg^{2+} removal (0-Mg^{2+}) enhanced presynaptic Ca^{2+} transients. This enhancement was blocked by extracellular APV. Top view is sample traces. Black indicates Ctrl, blue 0-Mg^{2+}. Bottom view is summary plots.

(E) Mg^{2+} removal enhanced presynaptic Ca^{2+} transients in the presence of intracellular MK801 (iMK801). Bottom image shows that 1 of 49 analyzed synaptic profiles had GluN1 labeling in the presynaptic active zone. Top view is sample traces. Black indicates Ctrl, blue 0-Mg^{2+}. Bottom view is summary plots.

(F) Complementary replica images were labeled for GluN1 with 5 nm gold particles (red) and CAST with 10 nm gold particles (black). Top images show that three presynaptic active zones with CAST labeling (left) have their complementary replica (arrows) without labeling for GluN1 on the presynaptic E face (right).

Columns represent the mean, circles the individual slices. Error bars, SEM. NS $p > 0.05$ and $*p < 0.05$. See also Figure S3.

Because the NMDAR-dependent enhancement of presynaptic Ca^{2+} transients can modulate the presynaptic release probability, we monitored changes in fEPSPs during five stimuli at 50 Hz. We hypothesized that activation of postsynaptic NMDARs during preceding multisynaptic EPSPs could trigger K^+ efflux and potentiate the succeeding EPSPs. Indeed, APV reduced the ratio between first and fifth fEPSPs in the train ($fEPSP_5$/$fEPSP_1$) to 85% ± 4.8% of Ctrl (n = 6; p = 0.58, Wilcoxon signed-rank test; Figure 5D) with no effect on the first fEPSP (101% ± 11.8% of baseline, n = 7; p > 0.05, Wilcoxon signed-rank test). However, APV had no effect on the $fEPSP_5$/$fEPSP_1$ ratio in CA1-GluN1 KO mice (107% ± 8.1% of baseline, n = 7; p = 0.66, Wilcoxon signed-rank test). These findings suggest that activation of postsynaptic NMDARs regulates presynaptic glutamate release in Schaffer collaterals in an activity-dependent manner. We further confirmed that this regulation is mediated by K^+ elevation in the synaptic cleft. An increase in extracellular K^+ is known to produce a biphasic effect of presynaptic release, first potentiation, and then depression (Hori and Takahashi, 2009). We increased extracellular K^+ to 7.5 mM, which potentiated fEPSPs to 144% ± 16% of baseline (n = 7; p < 0.05, Wilcoxon signed-rank test). In this condition, APV application produced no significant effect on $fEPSP_5$/$fEPSP_1$ ratio (100% ± 5% of baseline in 7.5 mM K^+, n = 8; p = 0.19, Wilcoxon signed-rank test),

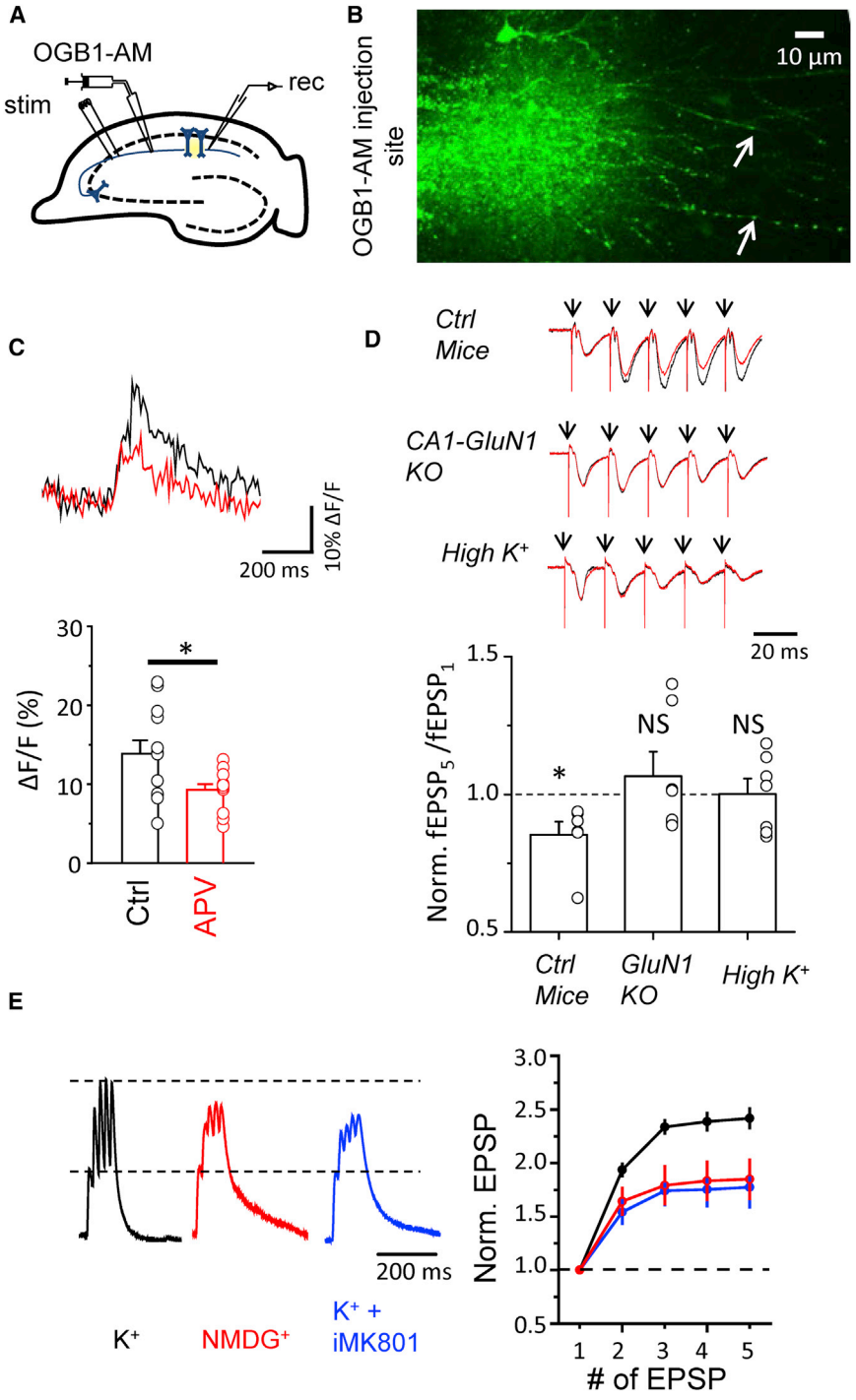

Figure 5. Activation of Multiple Synaptic Inputs Is Required for Regulation of Presynaptic Ca^{2+} Transients and Glutamate Release by Postsynaptic NMDARs

(A) Schematic illustrates the experimental arrangement for Ca^{2+} imaging in multiple boutons.

(B) Oregon green BAPTA1-AM was pressure injected into the *str.radiatum* to label presynaptic fibers (arrows).

(C) Presynaptic Ca^{2+} transients recorded in response to extracellular stimulation were sensitive to APV. Top view is sample traces in Ctrl (black) and in APV (red). Bottom view is a summary plot.

(D) APV reduced the $fEPSP_5/fEPSP_1$ ratio in response to 5× 50 Hz stimulation in Ctrl but not in CA1-GluN1 KO mice or at high K^+ (7.5 mM). Top views are sample traces in Ctrl (black) and in APV (red). Bottom view is a summary plot of APV effect. The $fEPSP_5/fEPSP_1$ ratio in APV is normalized to Ctrl.

(E) A 5 × 50 Hz stimulation enhanced the amplitude of subsequent EPSPs in a single neuron. This enhancement was suppressed by replacing postsynaptic K^+ for $NMDG^+$ or blockade of postsynaptic NMDARs by iMK801. Left view is sample traces of EPSPs produced by 5 × 50 Hz stimulation in Ctrl (black, K^+-based solution), with $NMDG^+$-based solution (red) and with iMK801 (blue, K^+-based solution with iMK801). Right view is EPSP amplitudes normalized to the amplitude of the first EPSP.

In (C) and (D), the columns represent the mean, circles the individual slices. Error bars, SEM. NS $p > 0.05$ and $^*p < 0.05$. Arrows indicate electrical stimulation.

suggesting that elevated K^+ occludes the effect of NMDAR-dependent K^+ efflux on the presynaptic terminal.

Next, we recorded EPSPs in current clamp mode in a single CA1 pyramidal neuron with KCH_3SO_3-based solution in the absence of all blockers (Figure 5E). Five stimuli at 50 Hz delivered to Schaffer collaterals triggered EPSPs with increasing amplitudes. The facilitation of EPSPs in the burst was significantly reduced when the recordings were performed with $NMDGMeSO_4$-based solution, which replaces intracellular K^+ and prevents K^+ efflux during synaptic transmission ($F(1,4) = 74.16$, $p < 0.001$ for the effect of EPSP facilitation during the burst; $F(1,4) = 11.04$, $p = 0.008$ for the effect of K^+ replacement for $NMDG^+$; $F(1,4) = 6.1$, $p < 0.001$ for interaction of facilitation effect and K^+ replacement; repeated-measures two-way ANOVA). The facilitation of EPSPs in the burst was also reduced when iMK801 was added to KCH_3SO_3-based solution ($F(1,4) = 6.46$, $p = 0.03$ for the difference between Ctrl and iMK801 solutions; $F(1,4) = 6.1$, $p < 0.001$ for interaction of facilitation effect and solution replacement; repeated-measures two-way ANOVA), suggesting that K^+ efflux through postsynaptic NMDARs plays the key role in presynaptic facilitation.

DISCUSSION

In this study, we found that the extracellular K^+ concentration in the synaptic environment increases following synaptic stimulation

and that this is in a large part due to K^+ efflux from postsynaptic NMDARs. Our results suggest that this increase in K^+ can act as a retrograde messenger modulating Ca^{2+} entry at presynaptic terminals.

Although extracellular K^+ rises during glutamatergic synaptic transmission have long been described (Bergles and Jahr, 1997; Poolos et al., 1987), the contribution of distinct synaptic glutamate receptors to K^+ efflux has not been investigated. We have found that postsynaptic NMDARs contribute substantially more to K^+ efflux than do AMPARs during stimulation of multiple Schaffer collaterals. Although synaptic AMPARs generate a greater peak current than do NMDARs, AMPARs activate and deactivate within a few milliseconds of presynaptic glutamate release. In contrast, the open probability of NMDARs typically peaks 20–30 ms postactivation and decays over hundreds of milliseconds (Attwell and Gibb, 2005). Moreover, NMDARs have relatively larger single-channel conductance compared to AMPARs (Spruston et al., 1995). Together, this makes the total electric charge carried by NMDARs on average five times larger than that of AMPARs during extracellular stimulation of Schaffer collaterals (Otmakhova et al., 2002). In addition, the contribution of NMDARs (which normally require AMPAR-dependent depolarization to activate) can be further increased by longer-lasting membrane depolarization during sustained postsynaptic activity, which could further relieve the receptor Mg^{2+} block. Such channel properties provide a potential explanation for the larger contribution of NMDARs to K^+ efflux and allow a sufficient time integration window for the buildup of local extracellular K^+ that could affect subsequent synaptic events.

We have found that K^+ efflux through postsynaptic NMDARs enhance presynaptic Ca^{2+} transients and activity-dependent fEPSP facilitation. The candidate underlying mechanism is presynaptic depolarization produced by extracellular K^+ rise (Hori and Takahashi, 2009). Depolarization of the presynaptic terminal can broaden AP time course (Geiger and Jonas, 2000; Hori and Takahashi, 2009; Sasaki et al., 2011) and boost presynaptic Ca^{2+} entry. In some excitatory hippocampal synapses, neurotransmitter release varies with presynaptic Ca^{2+} entry with a 2.5-power relationship (Scott et al., 2008), suggesting that even a minor change in presynaptic Ca^{2+} can have a significant impact on the magnitude of multisynaptic EPSCs.

Depolarization of the postsynaptic neuron enhances retrograde K^+ signaling not only by removing the voltage-dependent Mg^{2+} block of NMDARs but also by increasing the driving force for K^+. This could be another reason why strong postsynaptic depolarization resulting from the activation of multiple synaptic inputs is required for K^+-mediated retrograde signaling. Activation of a single axon does not produce sufficient postsynaptic depolarization to achieve either the necessary numbers of Mg^{2+}-unblocked NMDARs or the high K^+ driving force. This and related phenomena can explain an important distinction between two types of ionic retrograde signals mediated by NMDARs: the K^+ elevation described here and the Ca^{2+} depletion reported previously (Rusakov and Fine, 2003). The effects of intracleft Ca^{2+} depletion could occur at a single synapse, and its effect on release probability could only be detected within 8–20 ms postrelease because this phenomenon depends directly on the time course of intracleft Ca^{2+} (Rusakov and Fine, 2003). As measured from I_K, the extracellular K^+ rise lasts for hundreds of milliseconds and, thus, could increase presynaptic release probability above and beyond the effects mediated by partial Ca^{2+} depletion in the cleft.

Our data suggest that retrograde signaling due to NMDAR-dependent K^+ efflux requires relatively strong postsynaptic depolarization. How could this occur in physiological conditions? A recent study has shown that during network activity in situ, adjacent spines are frequently activated in synchrony, thus producing relatively strong postsynaptic depolarization: this corresponds to dendritic foci that receive locally convergent inputs from presynaptic cell assemblies (Takahashi et al., 2012). Synchronous activation of such clustered synaptic inputs can trigger generation of a local dendritic spike (Polsky et al., 2009), which also involves regenerative activation of NMDARs resulting from the voltage-dependent relief of Mg^{2+} block at 10–20 μm dendritic segments (Rhodes, 2006). Because the amplitudes of such dendritic spikes are much larger, and their spatial localization is more specific, than that of back-propagating APs (Golding et al., 1999), they appear a plausible candidate for triggering dendritic branch-specific retrograde K^+ signaling, especially in distal dendrites.

Retrograde K^+ signaling can also be linked to certain forms of synaptic plasticity. Facilitation of the retrograde K^+ signal by the coincidence of presynaptic release with a bAP may be important for spike time-dependent plasticity (STDP) (Abbott and Nelson, 2000; Bi and Poo, 1998). Sustained potentiation of EPSPs can also lead to increased postsynaptic K^+ efflux (Ge and Duan, 2007). Thus, long-term potentiation can be considered not only a mechanism to increase synaptic strength but also a mechanism to increase retrograde K^+ signaling. Because synaptic plasticity has been associated with learning and memory, further studies are needed to elucidate the role of enhanced NMDAR-mediated retrograde K^+ signaling in these brain functions.

Our findings also shed light on mechanisms underlying some forms of interactions within the tripartite synapse involving a local astrocyte. Ca^{2+} events in hippocampal astrocytes trigger release of D-serine, a coagonist of neuronal NMDARs (Henneberger et al., 2010; Panatier et al., 2006). D-serine can enhance NMDAR-mediated retrograde signaling by K^+, suggested by the finding that Ca^{2+} uncaging in hippocampal astrocytes produces local broadening of APs in axons of CA3 pyramidal neurons and facilitation of downstream synaptic transmission (Sasaki et al., 2011), which was prevented by a mixture of AMPAR and NMDAR antagonists.

In summary, our results propose that NMDAR-mediated K^+ retrograde signaling contributes to modulation of presynaptic neurotransmitter release and is therefore likely to be important for neuronal computation and plasticity. We identify the receptor that regulates synaptic K^+ efflux as the postsynaptic NMDAR, but further studies are needed to address the role of cleft geometry and K^+ clearance mechanisms for K^+ dynamics in the synaptic cleft.

EXPERIMENTAL PROCEDURES

Rats and Mice Experiments

All the experiments were done in 21- to 35-day-old Sprague-Dawley rats and 28- to 35-day-old C57BL/6J mice with two exceptions: (1) 42- to 49-day-old CA1-GluN1 KO mice (NR1 *fl/fl; CaMKII-Cre*) and littermate Ctrls (NR1 *fl/fl*)

(Tsien et al., 1996) were used for Figures 1I and 5D; and (2) 26-day-old rats, but no mice, were used for Figure 3F. When both rats and mice were used, no difference between species was found, and the results were grouped together. All procedures were done in accordance with the RIKEN regulations. Animals were anesthetized with 2-bromo-2-chloro-1,1,1-trifluroethane and decapitated.

Hippocampal Slice Preparation

The brain was exposed, chilled with ice-cold solution containing 75 mM sucrose, 87 mM NaCl, 2.5 mM KCl, 0.5 mM $CaCl_2$, 1.25 mM NaH_2PO_4, 7 mM $MgCl_2$, 25 mM $NaHCO_3$, 1 mM Na-ascorbate, and 11 mM D-glucose. Hippocampi from both hemispheres were isolated, then transverse slices (350–400 μm) were cut with a vibrating microtome (Microm HM 650V; Thermo Fisher Scientific) and left to recover for 30 min at 34°C and then at room temperature for 1 hr in an interfaced chamber with "storage" solution containing 127 mM NaCl, 2.5 mM KCl, 1.25 mM NaH_2PO_4, 1 mM $MgCl_2$, 1 mM $CaCl_2$, 25 mM $NaHCO_3$, and 25 mM D-glucose. Next, the slices were transferred to the recording chamber and were continuously perfused with a solution containing 127 mM NaCl, 2.5 mM KCl, 1.25 mM NaH_2PO_4, 1 mM $MgCl_2$, 2 mM $CaCl_2$, 25 mM $NaHCO_3$, and 25 mM D-glucose. All solutions were saturated with 95% O_2 and 5% CO_2. Osmolarity was 298 ± 3 mOsm. A total of 25 μM NBQX, 100 μM picrotoxin, 5 μM CGP52432, and 200 μM S-MCPG was added to the solution to block AMPA/kainate, $GABA_A$, $GABA_B$, and mGluRs, respectively, unless stated otherwise. In Ca^{2+}-free solution, 0.5 mM EGTA was added (Shah and Haylett, 2002). Cells were visually identified under infrared DIC using the Olympus BX-61 microscope.

Electrophysiology

Whole-cell recordings in CA1 *str.radiatum* astrocytes were obtained using patch electrodes filled with a solution containing 135 mM KCH_3SO_3, 10 mM HEPES, 10 mM Na_2-phosphocreatine, 4 mM $MgCl_2$, 4 mM Na_2ATP, and 0.4 mM NaGTP (pH adjusted to 7.2 with KOH; osmolarity to 290 mOsm) and with a resistance of 3–5 MΩ. Passive astrocytes were identified by small soma size (about 10 μm), low resting membrane potential (−84.0 ± 0.5 mV, n = 16,) and low input resistance (16.3 ± 1.4 MΩ, n = 16). Passive cell properties were confirmed by linear I–V characteristics (Figure 1A).

For simultaneous field potential recordings, the glass electrode filled with the extracellular solution was placed in the immediate vicinity of the recorded astrocytes. Synaptic responses were evoked by stimulation of Schaffer collaterals with a bipolar electrode (FHC) placed in the *str.radiatum* more than 200 μm from the recording site.

Whole-cell recordings in CA3 pyramidal neurons were obtained using patch electrodes filled with the solution containing 130 mM KCH_3SO_3, 8 mM NaCl, 10 mM HEPES, 10 mM Na_2-phosphocreatine, 0.4 mM Na_2GTP, 4 mM MgATP, and 3 mM Na-ascorbate (pH adjusted to 7.2 with KOH; osmolarity to 290 mOsm). APs were induced by somatic current injections (3 ms, 1–2 nA). The series resistance was usually <20 MΩ, and data were discarded if it changed by more than 20% during the recording. In current clamp mode, the series resistance was compensated with "bridge balance" function.

Whole-cell recordings in CA1 pyramidal neurons were obtained using patch electrodes filled with the solution containing 130 mM KCH_3SO_3, 8 mM NaCl, 10 mM HEPES, 2 mM EGTA, 10 mM Na_2-phosphocreatine, 0.4 mM Na_2GTP, 4 mM MgATP, 3 mM Na-ascorbate, and 10 mM QX314Cl (pH adjusted to 7.2 with KOH; osmolarity to 290 mOsm). In some cases, intracellular MK801 was added to the solution to block postsynaptic NMDARs; in other cases, KCH_3SO_3 was replaced for N-methyl-D-glucamine (NMDG) CH_3SO_3 to prevent postsynaptic K^+ efflux during synaptic transmission (Chen and Lipton, 1997).

The signals were recorded with the patch-clamp amplifier Multiclamp 700B (Molecular Devices), filtered at 2 kHz, and digitized at 4–10 kHz with the NI PCI-6221 card (National Instruments). The data were visualized and stored with the software WinWCP (supplied free of charge to academic users by Dr. John Dempster, University of Strathclyde, UK).

Ca^{2+} Imaging

Ca^{2+} dynamics in individual axons was studied in the cells filled through the patch pipette with Alexa Fluor 594 (50 μM) and Fluo-5F (200 μM) for at least 20 min before the start of recording. Two-photon Ca^{2+} imaging was performed with a two-scanner FV1000-MPE laser-scanning microscope (Olympus) equipped with a mode-locked (<140 fs pulse width) tunable 720–930 nm laser Chameleon XR (Coherent). Both dyes were excited at 810 nm laser wavelength, and their fluorescence was chromatically separated and detected with two independent photomultipliers (PMTs). Alexa Fluor 594 emission was used to identify the axonal boutons of CA3 pyramidal neurons (about 150 μm from the soma). Line-scan imaging was synchronized with electrophysiological recordings. The dark noises of the PMTs ($G_{dark\ noise}$ and $R_{dark\ noise}$) were collected when the laser shutter was closed in every recording. The changes in baseline Ca^{2+} level were monitored as a ratio between baseline Fluo-5F and Alexa Fluor 594 fluorescences throughout the experiment: $G/R = (G_{baseline} - G_{dark\ noise})/(R_{baseline} - R_{dark\ noise})$. If this ratio increased during the experiment by more than 20%, the cells were discarded. Ca^{2+} transients were presented as $\Delta G/R = (G_{peak} - G_{baseline})/(R_{baseline} - R_{dark\ noise})$, where $G_{baseline}$ and $R_{baseline}$ are averaged fluorescences 50–100 ms before the stimulation, and G_{peak} is the averaged fluorescences 30–40 ms around the peak fluorescence. Using high-frequency stimulation (30 stimuli × 100 Hz), we established that the Ca^{2+} dye was far from saturation (Figure S4). During the recordings, we also found that concentration of both dyes increases in the boutons (Figure S5). Diffusion of Ca^{2+} dyes introduces additional Ca^{2+} buffer, reducing the amplitude of recorded Ca^{2+} transients (Brenowitz and Regehr, 2007). Therefore, we established the mean amplitude of Ca^{2+} transients in Ctrl recordings (n = 5) without any pharmacological treatment. The points of recordings with pharmacological treatment were normalized to corresponding mean amplitudes obtained in Ctrl recordings.

Axonal Ca^{2+} dynamics in response to stimulation of multiple axons was performed after bolus loading of 500 μM Oregon green BAPTA1-AM dissolved in 2% Pluronic F-127 and 10% DMSO through the glass pipette. The tip of the pipette was inserted into CA1 *str.radiatum*, and the dye-containing solution was injected (50–60 hPa for 5 min) (Sasaki et al., 2011). After a recovery period of >1 hr in a recording chamber, confocal images were taken with a 488 nm argon laser (Melles Griot) and emission filter (BA505IF). The viability of dye-loaded slices was verified by monitoring fEPSPs in response to Schaffer collateral stimulation. Ca^{2+} transients in response to Schaffer collateral stimulation were recorded in line-scan mode from axonal boutons located ~200 μm away from the dye-loading site and presented as relative change in fluorescence of single-dye $\Delta F/F_0$.

NBQX was omitted in Ca^{2+}-imaging experiments to allow AMPARs to depolarize the postsynaptic cell and release Mg^{2+} block, except in the experiments with Mg^{2+}-free solution, when NBQX was present to prevent epileptic activity.

Mathematical Modeling

K^+ dynamics within the cleft was calculated in a model synapse consisting of two cylinders (pre- and the postsynaptic parts) with the identical radii of 300 nm (R_{syn}) and located opposite to each other with a cleft (δ) of 20 nm (Savtchenko et al., 2013). The model synapse was separated by a 200 nm space from neighboring structures. Glutamate (3,000 molecules) was released in the center of the presynaptic part opposing the postsynaptic density of a 200 nm radius (R_{psd}). AMPARs (N_{AMPA}, 50) and NMDARs (N_{NMDA}, 20) were scattered inside the postsynaptic density and had the single channel conductances of γ_{AMPA} = 10 pS and γ_{NMDA} = 50 pS, respectively. K^+ flowed from postsynaptic neurons through both NMDARs and AMPARs into the cleft and then to the extracellular space, changing the K^+ concentration inside and outside the cleft. At any discrete time, K^+ concentration was calculated inside the *i-th* ring of radius r_i and a width of *dr* using different diffusion equations inside ($r < R_{psd}$, Equation 1) and outside ($r > R_{psd}$, Equation 2) of postsynaptic density.

$$\frac{\partial [P]}{\partial t} = D\frac{1}{r}\frac{\partial}{\partial r}\left(r\frac{\partial [P]}{\partial r}\right) + \frac{N_{NMDA}\gamma_{NMDA} * f(V,Mg) * [O]_{NMDA}(E_m - E_{NMDA})}{F\ V} + \frac{N_{AMPA}\gamma_{AMPA}[O]_{AMPA}(E_m - E_{AMPA})}{F\ V}$$

$$[P]_{out} = 2.5\ mM$$

(Equation 1)

$$\frac{\partial [P]}{\partial t} = D \frac{1}{r} \frac{\partial}{\partial r} \left(r \frac{\partial [P]}{\partial r} \right), \qquad \text{(Equation 2)}$$

where $[P]$ is K^+ concentration, which is equal to $[P]_{out}$ without receptor activation, D = 1 μm^2/ms is K^+ diffusion coefficient, $[O]_{NMDA}$ and $[O]_{AMPA}$ are the proportions of open NMDARs and AMPARs, respectively (see below), F is the Faraday constant, $V = \pi \delta R_{psd}^2$ is volume inside the cleft, and $f(V_p, Mg)$ is the function that determines voltage and Mg^{2+} dependence of NMDARs (Equation 3) (Jahr and Stevens, 1990).

$$f(V_p, Mg) = \frac{1}{1 + \frac{2[Mg^{2+}]}{3.57} Exp(-0.062 * V_p)}, \qquad \text{(Equation 3)}$$

where postsynaptic membrane potential inside the cleft (V_p) was calculated as

$$C_m \frac{dV_p}{dt} = I_p \quad \text{where} \quad I_p = G_m (V_p - V_r) + G_{NMDA} V_p + G_{AMPA} V_p, \qquad \text{(Equation 4)}$$

where V_r is the membrane potential outside the cleft, and I_p is the postsynaptic current that was calculated at each time step (dt, 0.1 μs).

$[O]_{NMDA}$ and $[O]_{AMPA}$ were calculated as previously described by Jonas (1993) and Lester et al. (1993) using the glutamate concentration ([Glu]) and the concentration of NMDARs

$$\left(\frac{N_{NMDA}}{(\pi R_{psd})^2} \right)$$

and AMPARs

$$\left(\frac{N_{AMPA}}{(\pi R_{psd})^2} \right)$$

in the postsynaptic density. [Glu] was modeled as a time-dependent dynamic process that corresponded to the solution of diffusion equation

$$[Glu] = [Glu]_{Init}|_{r=0} \frac{Exp\left(-\frac{r^2}{4 D_{Glu} t} \right)}{4 \pi D_{Glu} t}, \qquad \text{(Equation 5)}$$

with initial glutamate concentration ($[Glu]_{init}$) inside the volume with radius $R_{psd}/10$

$$[Glu]_{Init}|_{r=0} = \frac{Q}{2\ \pi (0.1 R_{psd})^2 \delta N_A}, \qquad \text{(Equation 6)}$$

where N_A is the Avogadro number, D_{Glu} = 0.3 μm^2/ms is a diffusion coefficient inside the cleft (Savtchenko and Rusakov, 2005), and t is time.

The total number of potassium molecules inside the cleft at given time *t* was calculated as

$$2\pi \int_0^{Rsyn} r[P]\, dr. \qquad \text{(Equation 7)}$$

The model parameters were adjusted for 33°C–35°C. The model code was implemented in Mathematica 8.

SDS-FRL

The rats (26 days old) were anesthetized with sodium pentobarbital (50 mg/kg, i.p.) and perfused transcardially with 25 mM sodium phosphate buffer (PB) containing 0.15 M saline for 1 min, followed by perfusion with 2% paraformaldehyde in 0.1 M sodium PB for 12 min. Coronal slices (150 μm thick) were cut using a vibrating microslicer (Linear Dosaka) in 0.1 M PB. The CA1 region of hippocampus was trimmed from the slices. The trimmed specimens were immersed in 30% glycerol/0.1 M PB for a cryoprotection at 4°C overnight and frozen by a high-pressure freezer (HPM010; BAL-TEC, Balzers). Frozen tissues were then fractured at −140°C using a double-replica device and replicated by deposition of carbon (1–2 nm thick), platinum (uni-direction from 60°, 2 nm), and carbon (20 nm) in a freeze-fracturing device (JFDII; JEOL). Both sides of the complementary replicas were picked up individually, and the tissue that remained beneath the replicas was dissolved with gentle reciprocal shaking at 80°C for 18 hr in a solution containing 2.5% SDS, 20% sucrose, and 15 mM Tris-HCl (pH 8.3). The replicas were then washed in 50 mM Tris-buffered saline (TBS) (pH 7.4) containing 0.05% BSA and 0.05% normal goat serum (NGS) and blocked with 5% BSA plus 5% NGS in TBS for 1 hr at room temperature. The replicas were incubated with a mouse antibody against GluN1 (MAB363; 4 μg/ml, Millipore) together with a rabbit antibody against CAST (1:50 diluted; Hagiwara et al., 2005) at 15°C for 22 hr. Specimens were washed, then incubated with a mixture of anti-mouse antibodies conjugated with 5 nm gold particles (Amersham Pharmacia) and anti-rabbit antibodies conjugated with 10 nm gold particles (British Biocell International) for 29 hr at 15°C. The specificity of the NR1 antibody and CAST antibody was confirmed in our previous studies, respectively (Hagiwara et al., 2005; Tarusawa et al., 2009). Complementary replicas were examined at 100 kV with a Tecnai 12 transmission electron microscope (FEI Company). All images were photographed as stereo pairs having an 8° included angle and examined stereoscopically to exclude technical noise of the labeling for the data collections (Li et al., 2008). For further details regarding the drugs and chemicals used and data analysis, please refer to the Supplemental Experimental Procedures.

SUPPLEMENTAL INFORMATION

Supplemental Information includes Supplemental Experimental Procedures and five figures and can be found with this article online at http://dx.doi.org/10.1016/j.celrep.2013.10.026.

ACKNOWLEDGMENTS

The study was supported by The Ministry of Education and Science of the Russian Federation, project 14.B37.21.0852.

Received: June 27, 2012
Revised: September 3, 2013
Accepted: October 16, 2013
Published: November 21, 2013

REFERENCES

Abbott, L.F., and Nelson, S.B. (2000). Synaptic plasticity: taming the beast. Nat. Neurosci. Suppl. *3*, 1178–1183.

Attwell, D., and Gibb, A. (2005). Neuroenergetics and the kinetic design of excitatory synapses. Nat. Rev. Neurosci. *6*, 841–849.

Bergles, D.E., and Jahr, C.E. (1997). Synaptic activation of glutamate transporters in hippocampal astrocytes. Neuron *19*, 1297–1308.

Bi, G.Q., and Poo, M.M. (1998). Synaptic modifications in cultured hippocampal neurons: dependence on spike timing, synaptic strength, and postsynaptic cell type. J. Neurosci. *18*, 10464–10472.

Brenowitz, S.D., and Regehr, W.G. (2007). Reliability and heterogeneity of calcium signaling at single presynaptic boutons of cerebellar granule cells. J. Neurosci. *27*, 7888–7898.

Chen, H.S., and Lipton, S.A. (1997). Mechanism of memantine block of NMDA-activated channels in rat retinal ganglion cells: uncompetitive antagonism. J. Physiol. *499*, 27–46.

Contractor, A., Mulle, C., and Swanson, G.T. (2011). Kainate receptors coming of age: milestones of two decades of research. Trends Neurosci. *34*, 154–163.

Corlew, R., Wang, Y., Ghermazien, H., Erisir, A., and Philpot, B.D. (2007). Developmental switch in the contribution of presynaptic and postsynaptic NMDA receptors to long-term depression. J. Neurosci. *27*, 9835–9845.

Ge, W.P., and Duan, S. (2007). Persistent enhancement of neuron-glia signaling mediated by increased extracellular K+ accompanying long-term synaptic potentiation. J. Neurophysiol. *97*, 2564–2569.

Geiger, J.R., and Jonas, P. (2000). Dynamic control of presynaptic Ca(2+) inflow by fast-inactivating K(+) channels in hippocampal mossy fiber boutons. Neuron *28*, 927–939.

Gereau, R.W., 4th, and Conn, P.J. (1995). Multiple presynaptic metabotropic glutamate receptors modulate excitatory and inhibitory synaptic transmission in hippocampal area CA1. J. Neurosci. *15*, 6879–6889.

Golding, N.L., Jung, H.Y., Mickus, T., and Spruston, N. (1999). Dendritic calcium spike initiation and repolarization are controlled by distinct potassium channel subtypes in CA1 pyramidal neurons. J. Neurosci. *19*, 8789–8798.

Hagiwara, A., Fukazawa, Y., Deguchi-Tawarada, M., Ohtsuka, T., and Shigemoto, R. (2005). Differential distribution of release-related proteins in the hippocampal CA3 area as revealed by freeze-fracture replica labeling. J. Comp. Neurol. *489*, 195–216.

Henneberger, C., Papouin, T., Oliet, S.H., and Rusakov, D.A. (2010). Long-term potentiation depends on release of D-serine from astrocytes. Nature *463*, 232–236.

Hori, T., and Takahashi, T. (2009). Mechanisms underlying short-term modulation of transmitter release by presynaptic depolarization. J. Physiol. *587*, 2987–3000.

Ichinose, T., Yu, S., Wang, X.Q., and Yu, S.P. (2003). Ca2+-independent, but voltage- and activity-dependent regulation of the NMDA receptor outward K+ current in mouse cortical neurons. J. Physiol. *551*, 403–417.

Jahr, C.E., and Stevens, C.F. (1990). Voltage dependence of NMDA-activated macroscopic conductances predicted by single-channel kinetics. J. Neurosci. *10*, 3178–3182.

Jonas, P. (1993). AMPA-type glutamate receptors—nonselective cation channels mediating fast excitatory transmission in the CNS. EXS *66*, 61–76.

Krebs, C., Fernandes, H.B., Sheldon, C., Raymond, L.A., and Baimbridge, K.G. (2003). Functional NMDA receptor subtype 2B is expressed in astrocytes after ischemia in vivo and anoxia in vitro. J. Neurosci. *23*, 3364–3372.

Krnjević, K., Morris, M.E., and Reiffenstein, R.J. (1982). Stimulation-evoked changes in extracellular K+ and Ca2+ in pyramidal layers of the rat's hippocampus. Can. J. Physiol. Pharmacol. *60*, 1643–1657.

Lester, R.A., Tong, G., and Jahr, C.E. (1993). Interactions between the glycine and glutamate binding sites of the NMDA receptor. J. Neurosci. *13*, 1088–1096.

Li, X., Kamasawa, N., Ciolofan, C., Olson, C.O., Lu, S., Davidson, K.G., Yasumura, T., Shigemoto, R., Rash, J.E., and Nagy, J.I. (2008). Connexin45-containing neuronal gap junctions in rodent retina also contain connexin36 in both apposing hemiplaques, forming bihomotypic gap junctions, with scaffolding contributed by zonula occludens-1. J. Neurosci. *28*, 9769–9789.

McGuinness, L., Taylor, C., Taylor, R.D., Yau, C., Langenhan, T., Hart, M.L., Christian, H., Tynan, P.W., Donnelly, P., and Emptage, N.J. (2010). Presynaptic NMDARs in the hippocampus facilitate transmitter release at theta frequency. Neuron *68*, 1109–1127.

Ngo-Anh, T.J., Bloodgood, B.L., Lin, M., Sabatini, B.L., Maylie, J., and Adelman, J.P. (2005). SK channels and NMDA receptors form a Ca2+-mediated feedback loop in dendritic spines. Nat. Neurosci. *8*, 642–649.

Nicholson, C., ten Bruggencate, G., Stöckle, H., and Steinberg, R. (1978). Calcium and potassium changes in extracellular microenvironment of cat cerebellar cortex. J. Neurophysiol. *41*, 1026–1039.

Otmakhova, N.A., Otmakhov, N., and Lisman, J.E. (2002). Pathway-specific properties of AMPA and NMDA-mediated transmission in CA1 hippocampal pyramidal cells. J. Neurosci. *22*, 1199–1207.

Panatier, A., Theodosis, D.T., Mothet, J.P., Touquet, B., Pollegioni, L., Poulain, D.A., and Oliet, S.H. (2006). Glia-derived D-serine controls NMDA receptor activity and synaptic memory. Cell *125*, 775–784.

Polsky, A., Mel, B., and Schiller, J. (2009). Encoding and decoding bursts by NMDA spikes in basal dendrites of layer 5 pyramidal neurons. J. Neurosci. *29*, 11891–11903.

Poolos, N.P., Mauk, M.D., and Kocsis, J.D. (1987). Activity-evoked increases in extracellular potassium modulate presynaptic excitability in the CA1 region of the hippocampus. J. Neurophysiol. *58*, 404–416.

Prince, D.A., Lux, H.D., and Neher, E. (1973). Measurement of extracellular potassium activity in cat cortex. Brain Res. *50*, 489–495.

Qiu, C., Johnson, B.N., and Tallent, M.K. (2007). K+ M-current regulates the transition to seizures in immature and adult hippocampus. Epilepsia *48*, 2047–2058.

Regehr, W.G., Carey, M.R., and Best, A.R. (2009). Activity-dependent regulation of synapses by retrograde messengers. Neuron *63*, 154–170.

Rhodes, P. (2006). The properties and implications of NMDA spikes in neocortical pyramidal cells. J. Neurosci. *26*, 6704–6715.

Rusakov, D.A., and Fine, A. (2003). Extracellular Ca2+ depletion contributes to fast activity-dependent modulation of synaptic transmission in the brain. Neuron *37*, 287–297.

Sasaki, T., Matsuki, N., and Ikegaya, Y. (2011). Action-potential modulation during axonal conduction. Science *331*, 599–601.

Savtchenko, L.P., and Rusakov, D.A. (2005). Extracellular diffusivity determines contribution of high-versus low-affinity receptors to neural signaling. Neuroimage *25*, 101–111.

Savtchenko, L.P., and Rusakov, D.A. (2007). The optimal height of the synaptic cleft. Proc. Natl. Acad. Sci. USA *104*, 1823–1828.

Savtchenko, L.P., Sylantyev, S., and Rusakov, D.A. (2013). Central synapses release a resource-efficient amount of glutamate. Nat. Neurosci. *16*, 10–12.

Schiller, J., Schiller, Y., and Clapham, D.E. (1998). NMDA receptors amplify calcium influx into dendritic spines during associative pre- and postsynaptic activation. Nat. Neurosci. *1*, 114–118.

Scott, R., Ruiz, A., Henneberger, C., Kullmann, D.M., and Rusakov, D.A. (2008). Analog modulation of mossy fiber transmission is uncoupled from changes in presynaptic Ca2+. J. Neurosci. *28*, 7765–7773.

Shah, M.M., and Haylett, D.G. (2002). K+ currents generated by NMDA receptor activation in rat hippocampal pyramidal neurons. J. Neurophysiol. *87*, 2983–2989.

Sorra, K.E., and Harris, K.M. (1993). Occurrence and three-dimensional structure of multiple synapses between individual radiatum axons and their target pyramidal cells in hippocampal area CA1. J. Neurosci. *13*, 3736–3748.

Spruston, N., Jonas, P., and Sakmann, B. (1995). Dendritic glutamate receptor channels in rat hippocampal CA3 and CA1 pyramidal neurons. J. Physiol. *482*, 325–352.

Sylantyev, S., Jensen, T.P., Ross, R.A., and Rusakov, D.A. (2013). Cannabinoid- and lysophosphatidylinositol-sensitive receptor GPR55 boosts neurotransmitter release at central synapses. Proc. Natl. Acad. Sci. USA *110*, 5193–5198.

Takahashi, N., Kitamura, K., Matsuo, N., Mayford, M., Kano, M., Matsuki, N., and Ikegaya, Y. (2012). Locally synchronized synaptic inputs. Science *335*, 353–356.

Tarusawa, E., Matsui, K., Budisantoso, T., Molnár, E., Watanabe, M., Matsui, M., Fukazawa, Y., and Shigemoto, R. (2009). Input-specific intrasynaptic arrangements of ionotropic glutamate receptors and their impact on postsynaptic responses. J. Neurosci. *29*, 12896–12908.

Tsien, J.Z., Huerta, P.T., and Tonegawa, S. (1996). The essential role of hippocampal CA1 NMDA receptor-dependent synaptic plasticity in spatial memory. Cell *87*, 1327–1338.

Walz, W. (2000). Role of astrocytes in the clearance of excess extracellular potassium. Neurochem. Int. *36*, 291–300.

Wu, Y.W., Grebenyuk, S., McHugh, T.J., Rusakov, D.A., and Semyanov, A. (2012). Backpropagating action potentials enable detection of extrasynaptic glutamate by NMDA receptors. Cell Rep. *1*, 495–505.